PHOTONICS Research

Dynamic generation of multiplexed vortex beams by a space-time-coding metasurface

Pengcheng Tang,[1] Liming Si,[1,*] Qianqian Yuan,[1] Jie Tian,[2] Jiaxuan Deng,[1] Tianyu Ma,[1] Xiue Bao,[1] Chong He,[2] and Weiren Zhu[2,3]

[1]Beijing Key Laboratory of Millimeter Wave and Terahertz Technology, School of Integrated Circuits and Electronics, Beijing Institute of Technology, Beijing 100081, China
[2]Department of Electronic Engineering, Shanghai Jiao Tong University, Shanghai 200240, China
[3]e-mail: weiren.zhu@sjtu.edu.cn
*Corresponding author: lms@bit.edu.cn

Received 1 October 2024; revised 31 October 2024; accepted 9 November 2024; posted 11 November 2024 (Doc. ID 543744); published 24 December 2024

Dynamic generation of multimode vortex waves carrying orbital angular momentum (OAM) utilizing programmable metasurfaces has attracted considerable attention. Yet, it is still a challenge to achieve multiplexed vortex waves with an arbitrary customized mode combination, stemming fundamentally from the discrete control over phase exhibited by current programmable metasurfaces, which are typically constrained to a limited 1-bit or 2-bit discrete resolution. In this paper, we propose, to our knowledge, a new strategy for dynamic generation of multiplexed vortex beams based on a space-time-coding metasurface, capable of quasi-continuous complex-amplitude modulation for harmonic waves. As a proof of concept, a metasurface prototype for generating multiplexed vortex beams with the customized mode composition and power allocation is established based on the transmissive space-time-coding meta-atoms regulated by the field programmable gate array controller. The mode purity of the vortex beams with a single OAM mode of +1, +2, and +3 generated by the metasurface is as high as over 0.93. The generated multiplexed vortex beams carrying (+1, +2, +3) OAM modes with a power ratio of 1:1:1, (+1, +2, +3) modes with a power ratio of 1:2:3, and (−2, −1, +1, +2) modes with a power ratio of 1:2:2:1 are further verified effectively. The proposed space-time-coding metasurface has great potential for OAM multiplexing communication systems.

https://doi.org/10.1364/PRJ.543744

1. INTRODUCTION

Recently, vortex beams with orbital angular momentum (OAM) have attracted enormous attention in the field of communications owing to the orthogonality among different OAM modes [1,2]. Different from the polarization-, frequency-, and time-division multiplexing, vortex beam multiplexing is one of the space-division multiplexing techniques [3,4], showing great prospects for the improvement of the channel capacity of wireless communication systems. On one hand, since the OAM modes are orthogonal with each other, each OAM mode of vortex beams could be an independent channel for a data stream to increase the multiplexing dimension, which has been distinguished as OAM-division multiplexing (OAM-DM) [5,6]. On the other hand, the different OAM modes could be used to encode the information directly, which has been distinguished as an OAM-shifting key (OAM-SK) [7,8]. The generation of vortex beams with multiplexed OAM modes is essential in the vortex beam multiplexing communication system, in which mode composition and power allocation are usually arbitrary and complex. The traditional methods of vortex beam generation include a spiral phase plate, circular antenna array, annular traveling wave antenna, spiral reflector [9–14], etc.

Owing to the powerful capabilities of electromagnetic wave manipulation [15–17], metasurfaces are gradually becoming a popular method for generating vortex beams with the advantages of simpler structure, simpler feed networks, smaller volume, and better performance compared with traditional methods. Various vortex beam generating metasurfaces have been proposed including reflection and transmission types [18–21], while, theoretically, the transmissive metasurfaces are more suitable for the high-purity vortex beam generation as the feed blockage could be avoided [22,23]. Furthermore, Li *et al.* [24] proposed a high-purity transmissive multiplexed vortex beam generating metasurface with complex-amplitude modulation based on the passive chiral meta-atoms. To realize dynamic wavefront modulation, reconfigurable metasurfaces incorporating active devices such as positive-intrinsic-negative

(PIN) diodes, varactor diodes, photoactive semiconductor materials, graphene, and vanadium dioxide are proposed [25–28]. Reconfigurable metasurfaces based on PIN diodes show great advantages in reducing the complexity and cost for dynamic vortex beam generation at microwaves and millimeter waves [29–32]. However, the vortex beams generated by the above-mentioned reconfigurable metasurface could only carry a single OAM mode at one time. It is still challenging to generate dynamic multiplexed vortex beams with the customized mode composition and power allocation.

As a new branch of reconfigurable metasurfaces, the space-time-coding metasurfaces exhibit great capability in modulating the harmonic components of electromagnetic waves by introducing an additional controllable time dimension [33–36]. Many novel physical phenomena and exciting applications associated with the space-time-coding metasurfaces have been studied, including Lorentz reciprocity, Doppler effect, frequency conversion, harmonic manipulation, and so on [37–42]. Moreover, the space-time-coding metasurfaces allow more precise regulation of electromagnetic wave compared with traditional reconfigurable metasurfaces. The desired complex-amplitude modulation of harmonic waves could be achieved by controlling the space-time-coding metasurfaces to switch cyclically according to a predesigned space-time-coding sequence. Relatively swift time-domain modulation speed is necessary for the realization of the space-time-coding metasurface. The PIN diode is a good candidate for the construction of the space-time-coding metasurface at microwaves and millimeter waves owing to its high response speed, while indium tin oxide (ITO), microelectromechanical systems (MEMS), and electro-optic (EO) polymer [43–45] may find applications in the practical construction at optical frequencies. The widely reported reconfigurable metasurfaces for wavefront manipulation are designed for the phase-only modulation ignoring amplitude imformation [46–48]. Due to the superposition of multi-mode vortex wavefronts, complex-amplitude distribution rather than phase-only distribution for the single-mode case on the mtasurface aperture is needed for the multiplexed vortex beam generation. The integrated metasurface for on-chip optical vortices and conventional OAM generation methods at microwave and even higher frequencies exhibit good performance with especially high robustness in OAM order upscaling [49–51], while the OAM modes are fixed once the physical structure or input excitation is determined. The space-time-coding metasurface provides an easily implementable method for dynamically regulating the OAM mode composition and power allocation of the generated multiplexed vortex beams without changing the physical structure or input excitation.

In this paper, a method for the dynamic multiplexed vortex beam generation by the complex-amplitude modulation of harmonic waves based on the space-time-coding metasurface is proposed. The designed space-time-coding metasurface is composed of the 1-bit phase tunable meta-atoms with high transmission working around 5 GHz. Through independently controlling the PIN diodes on each space-time-coding meta-atom to switch cyclically by the field programmable gate array (FPGA), incident linearly polarized waves could be modulated dynamically. As examples, the space-time-coding sequences for the single-mode and multiplexed vortex beams are designed to study the metasurface's performance of precise phase and complex-amplitude modulation, respectively. Furthermore, we specify the power distribution of different modes in the multiplexed vortex beams to study the metasurface's capability of generating vortex waves with complex power allocation. Both the calculations and measurements verify the high mode purity of the vortex beam generated by the proposed space-time-coding metasurface.

2. THEORY AND DESIGN

Figure 1 shows the conceptual illustration of the proposed space-time-coding metasurface for the dynamic multiplexed vortex beam generation. The metasurface is composed of several meta-atoms that serve as 1-bit phase coders. The coding

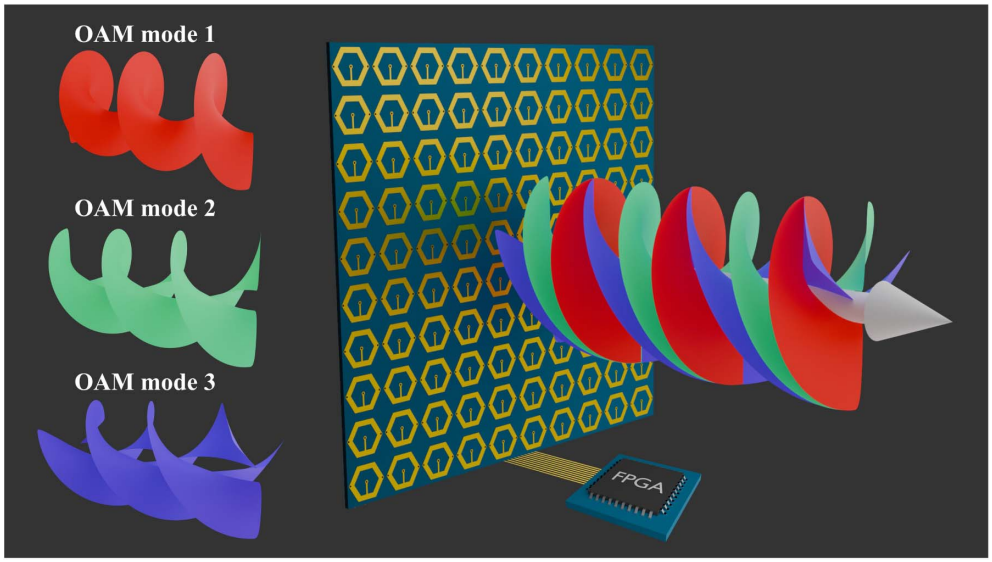

Fig. 1. Conceptual illustration of the proposed space-time-coding metasurface.

state of each meta-atom can be individually controlled by the FPGA. The quasi-continuous complex-amplitude modulation for +1st harmonic wave is achieved based on the space-time-coding method. Under the normal illumination of a linearly polarized plane wave, the transmitted wave could be converted into the multiplexed vortex beam with multiple different OAM modes by the metasurface. The mode composition and power allocation of the vortex beams could be dynamically regulated through changing the space-time-coding sequences.

As shown in Fig. 2, a metal hexagonal ring-shaped receiving-transmitting structure is adopted as the meta-atom. The period length of the meta-atom is p, composed of four copper (conductivity is 5.8×10^7 S/m) metal layers with the thickness of 0.035 mm and three dielectric substrates with the thicknesses of h_1, h_2, and h_3. The top layer shown in Fig. 2(b), consisting of two PIN diodes (Skyworks, SMP1320-079LF) arranged in the same direction and a metal ring, serves as the receiving layer responsible for receiving the incident plane wave linearly polarized along the y-axis direction. The bottom layer shown in Fig. 2(d), connected to the top layer by the metal via-hole, serves as the transmitting layer responsible for radiating the transmitted wave. The bias layer shown in Fig. 2(c) with two sector-shaped structures serving to isolate the high frequency signals is connected to the bottom layer by two metal via-holes. It should be noted that the metal ground is connected to the top layer but does not connect with the via-hole that links the top and bottom layers. The dielectric substrates on both sides are made of F4B (dielectric constant is 2.2, loss tangent is 0.001), while the bounding layer is made of Rogers RO4450F (dielectric constant is 3.52, loss tangent is 0.004). The detailed structural parameters and values of the meta-atom are presented in Table 1.

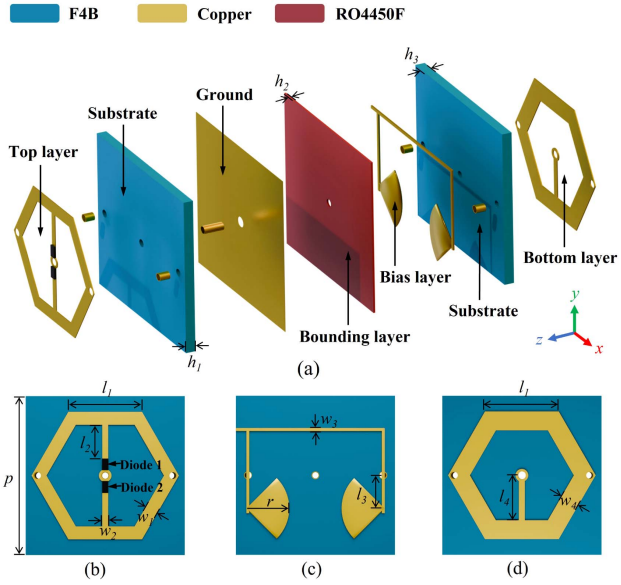

Fig. 2. Schematic diagram of the proposed meta-atom. (a) Exploded view of the meta-atom. Top view of (b) the top layer, (c) the bias layer, and (d) the bottom layer.

Full-wave simulations are performed in the commercial software CST Microwave Studio 2020 with the periodic boundary conditions set along the x- and y-axis directions. A y-polarized plane wave propagating along the $-z$-axis direction is set as the incident wave. The transmission coefficients from 4.5 to 5.4 GHz of the meta-atom are achieved with a frequency domain solver based on the finite element method (FEM). According to the states of the PIN diodes in the meta-atom, we define the state when Diode 1 is switched on and Diode 2 is switched off as State 0, and the state when Diode 1 is switched off and Diode 2 is switched on as State 1. The PIN diode Skyworks SMP1320-079LF could be equivalently modeled as a resistor-inductor-capacitor (RLC) series connection circuit with the parameters of inductance $L_{on} = 0.7$ nH, resistance $R_{on} = 0.2\,\Omega$ when switched on, and inductance $L_{off} = 0.5$ nH, capacitance $C_{off} = 0.24$ pF when switched off. Figures 3(a) and 3(b) plot the transmission amplitude T and phase ψ of the proposed meta-atom for State 0 and State 1, respectively. It can be observed from Fig. 3(a) that the transmission amplitude curves for both states almost overlap with each other. When the meta-atom is working in State 0, the transmission amplitude remains above 0.9 from 4.69 to 5.21 GHz, with a maximum value of 0.98. When the meta-atom is working in State 1, the transmission amplitude remains above 0.9 from 4.69 to 5.22 GHz, with a same maximum value of 0.98. As shown in Fig. 3(b), the transmission phase difference $\Delta\psi$ of the meta-atom between State 0 and State 1 remains stable at around 180° over a wide frequency band, exhibiting the 1-bit phase modulation performance. Owing to the advantages of stable and high transmission, along with the capability of 1-bit phase modulation, the proposed meta-atom is well-suited for the subsequent construction of efficient coding metasurfaces.

Traditional reconfigurable metasurfaces can only achieve discrete modulation of a single electromagnetic property, such as amplitude or phase, and it is difficult to meet the requirements for precise wavefront control to generate the multiplexed vortex beam with multiple different OAM modes. Time-coding metasurfaces have been proposed to tackle this issue, achieving simultaneous and quasi-continuous modulation of the amplitude and phase, namely, complex-amplitude modulation. According to the theory of a time-coding metasurface [35], the transmission coefficient can be defined as a linear combination of periodic pulse functions with a much slower time scale than that of incidence:

$$T(t) = \sum_{n=1}^{L} T^n U^n(t), \quad 0 < t < T_0, \tag{1}$$

in which L is the pulse number in a period, T^n is the time-coding transmission coefficient, and $U^n(t)$ is a periodic pulse function with the modulation period T_0:

Table 1. Detailed Structural Parameters and Values of the Meta-Atom

Parameter	p	r	l_1	l_2	l_3	l_4	w_1	w_2	w_3	w_4	h_1	h_2	h_3
Value (mm)	21	4.9	9.4	3.7	4	5.5	2	0.9	0.2	3	2	0.1	2

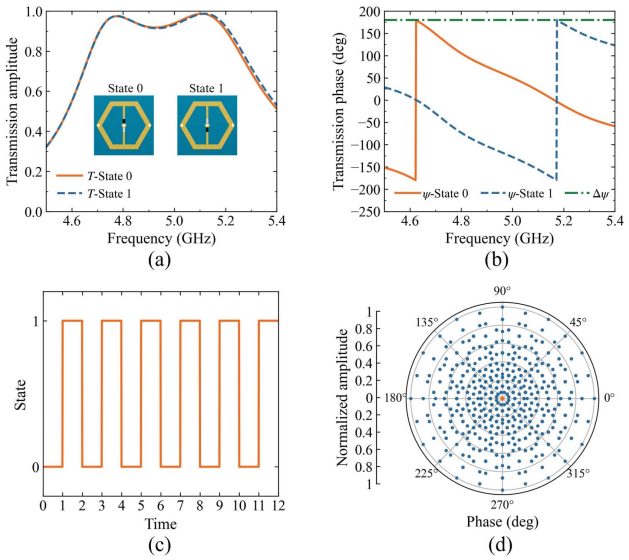

Fig. 3. (a) Transmission amplitude and (b) transmission phase of the proposed meta-atom. (c) Time-coding sequence of "010101010101". (d) All possible effective transmissions of +1st harmonic wave for time-coding sequences with periodic length $L = 12$.

$$U^n(t) = \begin{cases} 1, & (n-1)\tau \le t \le n\tau \\ 0, & \text{otherwise} \end{cases}, \tag{2}$$

where τ is the pulse width. We decompose $T(t)$ into the superposition of harmonic components according to the Fourier series expansion

$$T(t) = \sum_{m=-\infty}^{+\infty} a^m \exp(j2\pi m f_0 t), \tag{3}$$

where $f_0 = 1/T_0$ is the modulation frequency, m is the order of harmonic frequency, and harmonic components a^m are given by

$$a^m = \sum_{n=1}^{L} \frac{T^n}{L} \operatorname{sinc}\left(\frac{\pi \mathrm{m}}{L}\right) \exp\left[\frac{-j\pi m(2n-1)}{L}\right]. \tag{4}$$

From Eq. (4), we could infer the modulation of transmission harmonic components could be achieved by regulating the pulse number L and the time-coding transmission coefficient $T(t)$, namely, time-coding sequence.

The proposed metasurface is modulated by the time-coding sequence with $L = 12$. As an example, an $L = 12$ time-coding sequence "010101010101" where 0 and 1 represent State 0 and State 1 of the meta-atom is illustrated in Fig. 3(c). According to Eq. (4), one single time-coding sequence leads to one corresponding effective transmission performance. We calculate the effective transmission coefficients for the time-coding sequences including "000000000000"-"111111111111" using Eq. (4). Figure 3(d) shows all calculated possible effective transmissions of the +1st ($m = 1$) harmonic wave for time-coding sequences with periodic length $L = 12$ in a polar coordinate. The orange dot in Fig. 3(d) represents the transmission amplitude of 0 and transmission phase of 0 corresponding to the time-coding sequence "010101010101". It can be seen that the quasi-continuous modulation of the +1st harmonic wave's complex-amplitude is achieved theoretically based on the proposed time-coding metasurface. Then, time-coding sequences are established to construct the vortex beam generating metasurface.

The spatial phase distribution of the vortex beam with OAM can be expressed as $\exp(jl\phi)$, where ϕ is the azimuthal angle, and l is the topological charge or mode number of the corresponding OAM. The metasurface that constitutes the vortex beam generation needs to satisfy the transmission phase at position (x, y) of the array with the following equation:

$$\theta(x, y) = l \cdot \arctan\left(\frac{y}{x}\right). \tag{5}$$

The proposed metasurface is composed of 10×10 meta-atoms, with an overall size of 210 mm × 210 mm. The state of each meta-atom is independently governed by the time-coding sequences. Figures 4(a)–4(c) show the spatially discretized phase distribution of the metasurfaces for generating vortex beams with +1, +2, and +3 OAM modes, respectively. Mode purity is a key parameter for evaluating the quality of the vortex beam. In fact, the mode purity of the vortex beam with OAM generated by the metasurfaces is impacted by the following two reasons to some extent, including the limited overall array aperture and the coding of the continuous phase distribution into several discrete phase levels. Owing to the quasi-continuous modulation of the +1st harmonic wave's complex-amplitude achieved based on the proposed time-coding metasurfaces, it is possible to generate single-mode vortex beams with high mode purity despite using the proposed metasurface with a small aperture of only 10×10 meta-atoms ($\sim 3.5\lambda \times 3.5\lambda$).

For the generation of the multiplexed vortex beam with multiple different OAM modes of topological charges l_n and powers P_n, the complex-amplitude distribution rather than phase-only distribution for the single-mode case of the metasurface at position (x, y) is needed:

$$A(x, y) = \sum_{n=1}^{N} \sqrt{P_n} \exp\left[jl_n \cdot \arctan\left(\frac{y}{x}\right)\right]. \tag{6}$$

Figures 4(d) and 4(g) show the spatially discretized amplitude and phase distribution of the metasurface for generating the multiplexed vortex beam with three OAM modes of $(l_1, l_2, l_3, P_1{:}P_2{:}P_3) = (+1, +2, +3, 1{:}1{:}1)$, respectively. Furthermore, the complex-amplitude distribution of the metasurface for generating the multiplexed vortex beam with non-uniform power allocated OAM modes is studied, with Figs. 4(e) and 4(h) illustrating that of $(l_1, l_2, l_3, P_1{:}P_2{:}P_3) = (+1, +2, +3, 1{:}2{:}3)$ and Figs. 4(f) and 4(i) illustrating that of $(l_1, l_2, l_3, l_4, P_1{:}P_2{:}P_3{:}P_4) = (-2, -1, +1, +2, 1{:}2{:}2{:}1)$, respectively.

Then, we pick up the most matching time-coding sequences for each meta-atom locally according to the spatial amplitude and phase distribution for the vortex beam generation. By combining the independent time-coding for each meta-atom and the global space-coding for the metasurface, the space-time-coding metasurface is finally constructed. Figure 5 shows the space-time-coding sequences for generating the vortex beam

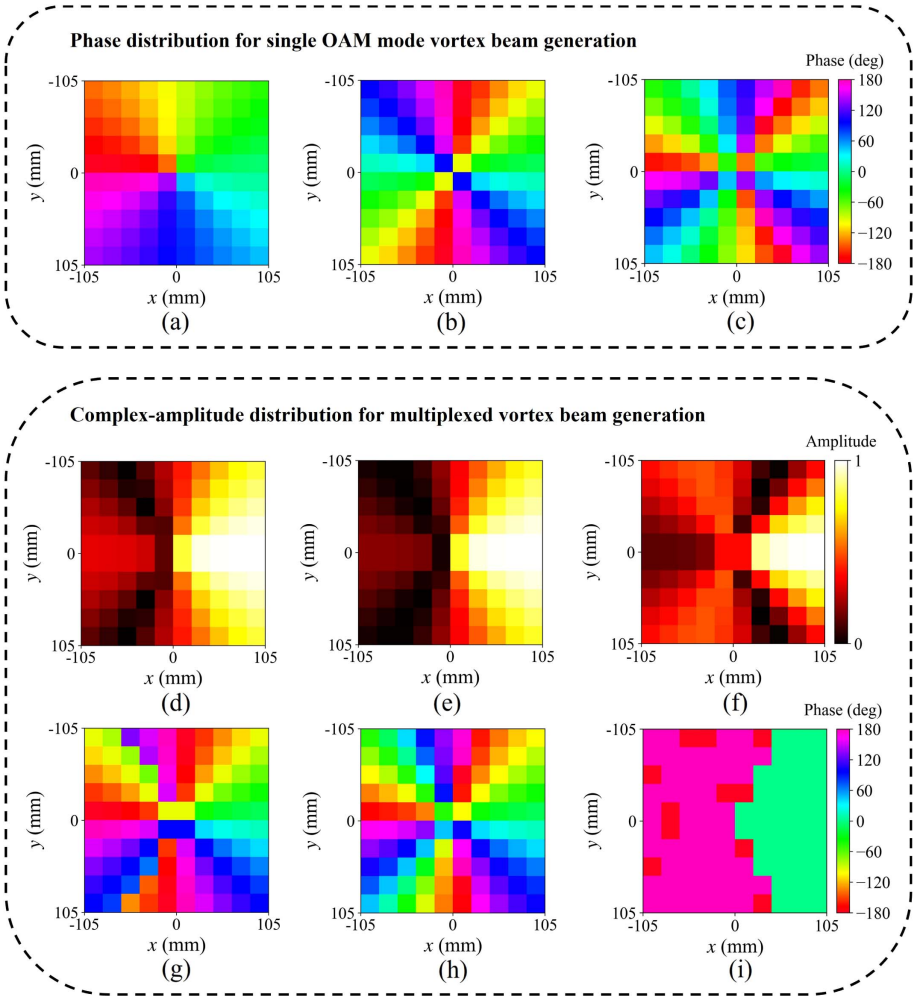

Fig. 4. Phase distribution of the metasurfaces for generating the vortex beam with (a) +1, (b) +2, and (c) +3 OAM mode. Amplitude distribution of the metasurfaces for generating the multiplexed vortex beam with OAM modes of (d) $(l_1, l_2, l_3, P_1{:}P_2{:}P_3) = (+1, +2, +3, 1{:}1{:}1)$, (e) $(l_1, l_2, l_3, P_1{:}P_2{:}P_3) = (+1, +2, +3, 1{:}2{:}3)$, and (f) $(l_1, l_2, l_3, l_4, P_1{:}P_2{:}P_3{:}P_4) = (-2, -1, +1, +2, 1{:}2{:}2{:}1)$, respectively. Phase distribution of the metasurfaces for generating the multiplexed vortex beam with OAM modes of (g) $(l_1, l_2, l_3, P_1{:}P_2{:}P_3) = (+1, +2, +3, 1{:}1{:}1)$, (h) $(l_1, l_2, l_3, P_1{:}P_2{:}P_3) = (+1, +2, +3, 1{:}2{:}3)$, and (i) $(l_1, l_2, l_3, l_4, P_1{:}P_2{:}P_3{:}P_4) = (-2, -1, +1, +2, 1{:}2{:}2{:}1)$, respectively.

with OAM modes of +1, +2, +3, $(l_1, l_2, l_3, P_1{:}P_2{:}P_3) = (+1, +2, +3, 1{:}1{:}1)$, $(l_1, l_2, l_3, P_1{:}P_2{:}P_3) = (+1, +2, +3, 1{:}2{:}3)$, and $(l_1, l_2, l_3, l_4, P_1{:}P_2{:}P_3{:}P_4) = (-2, -1, +1, +2, 1{:}2{:}2{:}1)$, respectively. We choose 5 GHz as the foundation frequency of the metasurface. The 5 GHz bands are the popular bands for new wireless applications and services such as Wi-Fi and cellular communication, owing to their favorable propagation characteristics and rich spectrum resources [52]. The time-coding modulation frequency f_0 is set as 50 kHz, leading to a frequency shift of 50 kHz for the +1st harmonic frequency (5 GHz + 50 kHz). Dynamic vortex beam generation is achieved through changing the space-time-coding sequences.

The near-field diffraction pattern of the metasurface can be derived by the Rayleigh-Sommerfeld formula

$$E(x, y, z) = \frac{d}{j\lambda} \int\int_{s'} E'(x', y', z') \frac{\exp(jk|r|)}{|r|^2} \mathrm{d}s', \quad (7)$$

where E and E' are the complex-amplitude distributions of the near-field at the observation plane and the metasurface, d is the distance between the observation plane and the metasurface, λ is the working wavelength, k is the wave number ($k = 2\pi/\lambda$), and r is the vector from (x, y, z) to (x', y', z'). Figure 6 illustrates the theoretical near-field amplitude and phase distributions of the +1st harmonic wave at the observation plane (located at 300 mm in front of the metasurface with an area of 800 mm × 800 mm) corresponding to the vortex beams generated by the proposed space-time-coding metasurface. The intensity profiles of the amplitude with a hollow center and the vortex-shaped phase wavefronts can be identified in Figs. 6(a)–6(c), indicating the typical characteristic of the vortex beam with a single OAM mode. Moreover, the intensity profiles of the amplitude increase with the OAM mode order, which is due to the fact that the divergence angle of the vortex beam enlarges as the OAM mode order increases, while it is difficult to intuitively find patterns in the amplitude and phase

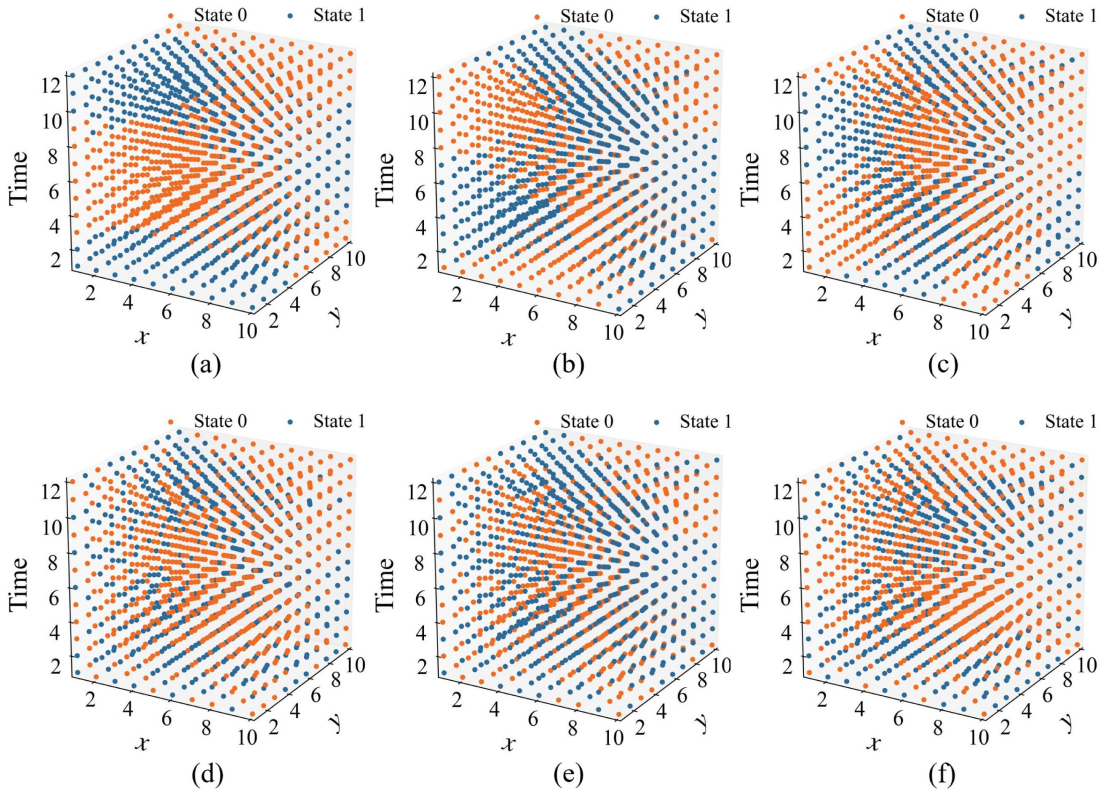

Fig. 5. Space-time-coding sequences for generating the vortex beam with OAM modes of (a) +1, (b) +2, (c) +3, (d) $(l_1, l_2, l_3, P_1{:}P_2{:}P_3) = (+1, +2, +3, 1{:}1{:}1)$, (e) $(l_1, l_2, l_3, P_1{:}P_2{:}P_3) = (+1, +2, +3, 1{:}2{:}3)$, and (f) $(l_1, l_2, l_3, l_4, P_1{:}P_2{:}P_3{:}P_4) = (-2, -1, +1, +2, 1{:}2{:}2{:}1)$, respectively.

distribution of the multiplexed vortex beams shown in Figs. 6(d)–6(f), due to the interference of different OAM modes. Therefore, we subsequently calculate the mode purity to quantitatively analyze the quality of the generated multiplexed vortex beams.

3. EXPERIMENTAL VERIFICATION

To verify the effectiveness of the space-time-coding metasurface for dynamic multiplexed vortex beam generation, the prototype metasurface with 10 × 10 meta-atoms shown in Fig. 7(a) is fabricated by the standard printed circuit board (PCB) technique.

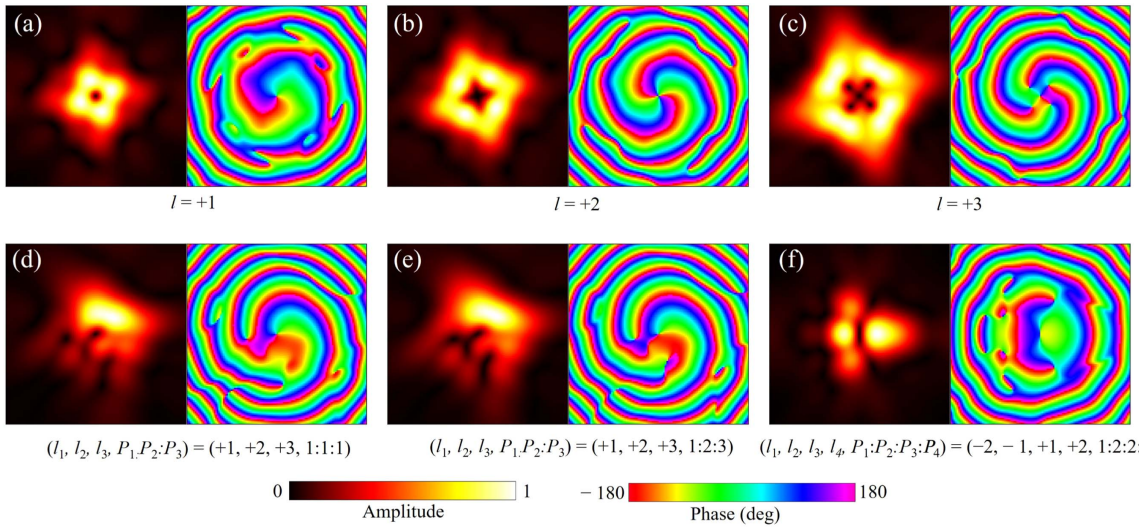

Fig. 6. The theoretical near-field amplitude and phase distribution for the vortex beams with OAM modes of (a) +1, (b) +2, (c) +3, (d) $(l_1, l_2, l_3, P_1{:}P_2{:}P_3) = (+1, +2, +3, 1{:}1{:}1)$, (e) $(l_1, l_2, l_3, P_1{:}P_2{:}P_3) = (+1, +2, +3, 1{:}2{:}3)$, and (f) $(l_1, l_2, l_3, l_4, P_1{:}P_2{:}P_3{:}P_4) = (-2, -1, +1, +2, 1{:}2{:}2{:}1)$, respectively.

As shown in Fig. 7(b), each meta-atom is connected to an independent FPGA's serial port via an independent feed line drawn from the bias layer. To ensure the PIN diodes in the meta-atom are forward biased as expected, 800 Ω resistors are used to adjust the current. A 1.65 V direct current (DC) power supply is connected to the ground plane of the proposed metasurface. Each serial port of the FPGA supports two output voltage states, 0 V and 3.3 V, enabling the switching between State 0 and State 1 of each meta-atom. The modulation period T_0 of the time-coding sequences provided by the FPGA is 20 μs with the modulation frequency $f_0 = 50$ kHz.

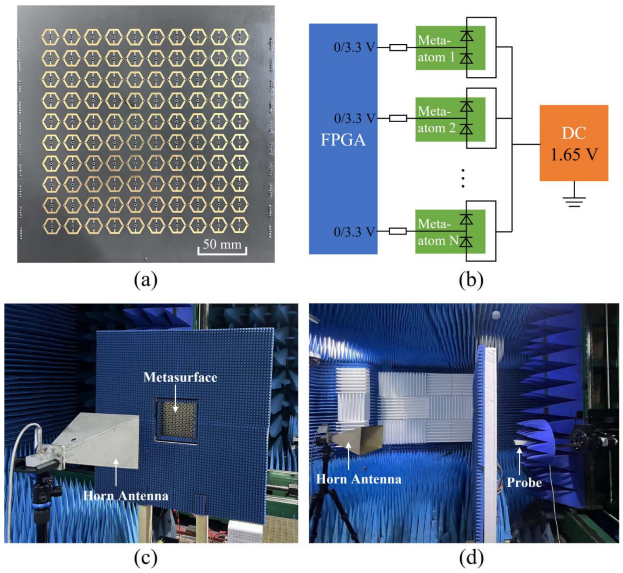

Fig. 7. (a) Photograph of the prototype space-time-coding metasurface. (b) Schematic diagram of the control circuit. (c), (d) Near-field experiment environment.

Figures 7(c) and 7(d) show the near-field experiment environment for the measurement of the proposed matasurface. A 20 dBi high-gain horn antenna connected to a microwave signal generator is placed 1000 mm away from the metasurface as the excitation source. The wavefront of the horn is approximately an equal-phase plane at this distance, allowing the excitation to be approximated as a plane wave. The metasurface is surrounded by the absorbers to reduce the diffraction of the excitation, which may influence the experimental results. The probe connected to the vector network analyzer is positioned 300 mm away from the metasurface, with a scan range of 800 mm × 800 mm.

Figure 8 illustrates the measured near-field amplitude and phase distributions of the +1st harmonic wave. These distributions correspond to the vortex beams generated by the proposed space-time-coding metasurface. The intensity profiles of the amplitude with a hollow center and the spiral phase fronts depicted in Figs. 8(a)–8(c) are clearly exhibited for the vortex beams with a single OAM mode. The measured amplitude distributions for the multiplexed vortex beam exhibit irregular patterns as shown in Figs. 8(d)–8(f). The phase distributions show an interaction of the spiral phases of the multiple OAM modes. In general, the measurement results are in good agreement with those theoretically derived by the diffraction formula.

The powers of different OAM modes could be obtained by

$$P_l = \frac{1}{2\pi}\int_0^{\infty}\left|\int_0^{2\pi} u(x,y)\cdot\exp(-jl\phi)\mathrm{d}\phi\right|^2 r\mathrm{d}r, \tag{8}$$

where $u(x,y)$ is the near-field complex-amplitude distribution. Then, the mode purity of each OAM mode can be calculated:

$$\eta_l = \frac{P_l}{\sum_{q=-\infty}^{+\infty} P_q}. \tag{9}$$

Figure 9 shows the comparison between theoretical and measured mode purity of the vortex beams generated by the proposed space-time-coding metasurface. The measured mode purities of the vortex beams with a single OAM mode of +1,

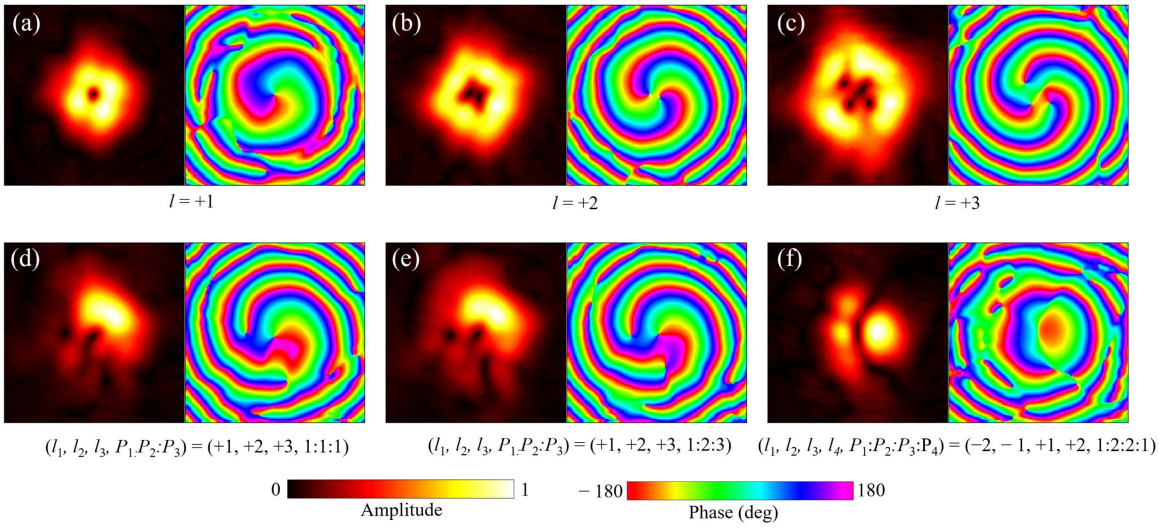

Fig. 8. The measured near-field amplitude and phase distribution for the vortex beams with OAM modes of (a) +1, (b) +2, (c) +3, (d) $(l_1, l_2, l_3, P_1{:}P_2{:}P_3) = (+1, +2, +3, 1{:}1{:}1)$, (e) $(l_1, l_2, l_3, P_1{:}P_2{:}P_3) = (+1, +2, +3, 1{:}2{:}3)$, and (f) $(l_1, l_2, l_3, l_4, P_1{:}P_2{:}P_3{:}P_4) = (-2, -1, +1, +2, 1{:}2{:}2{:}1)$, respectively.

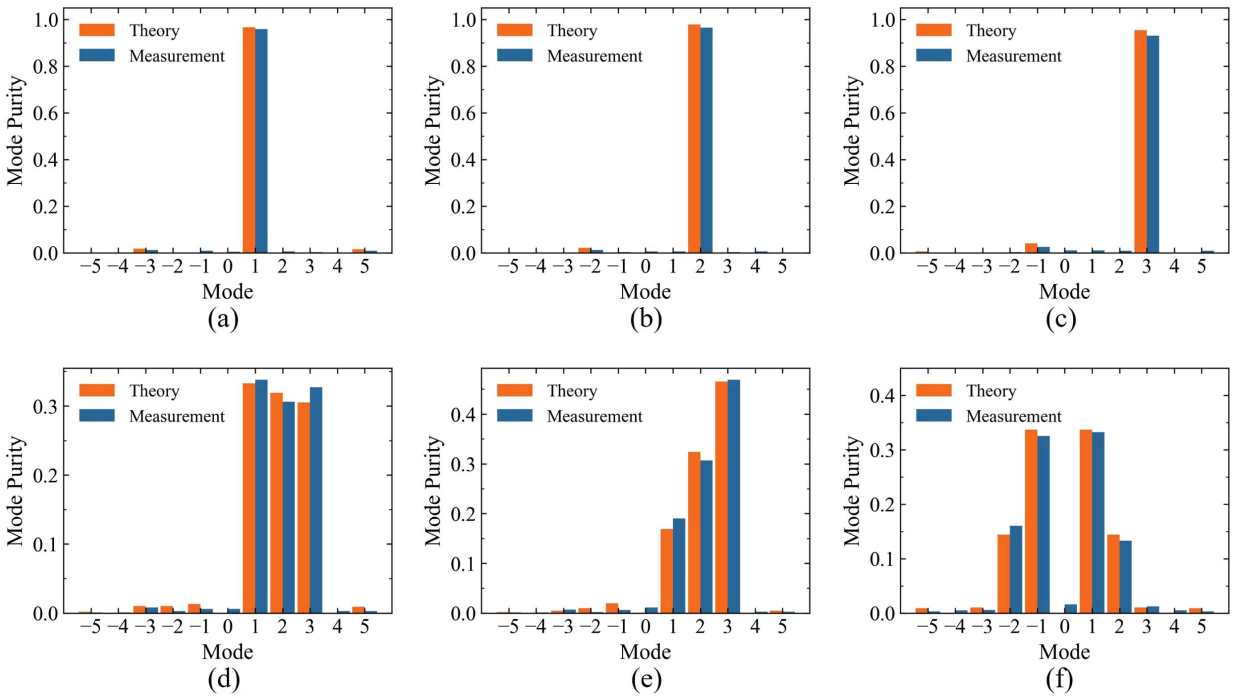

Fig. 9. The comparison between theoretical and measured mode purities of the vortex beams with OAM modes of (a) +1, (b) +2, (c) +3, (d) $(l_1, l_2, l_3, P_1{:}P_2{:}P_3) = (+1, +2, +3, 1{:}1{:}1)$, (e) $(l_1, l_2, l_3, P_1{:}P_2{:}P_3) = (+1, +2, +3, 1{:}2{:}3)$, and (f) $(l_1, l_2, l_3, l_4, P_1{:}P_2{:}P_3{:}P_4) = (-2, -1, +1, +2, 1{:}2{:}2{:}1)$, respectively.

+2, +3 are 0.959, 0.965, and 0.930, and the corresponding theoretical mode purities are 0.967, 0.979, and 0.954, respectively. The measured mode purities of the multiplexed vortex beams with OAM modes of $(l_1, l_2, l_3, P_1{:}P_2{:}P_3) = (+1, +2, +3, 1{:}1{:}1)$, $(l_1, l_2, l_3, P_1{:}P_2{:}P_3) = (+1, +2, +3, 1{:}2{:}3)$, and $(l_1, l_2, l_3, l_4, P_1{:}P_2{:}P{:}P_4) = (-2, -1, +1, +2, 1{:}2{:}2{:}1)$ are $(\eta_1{:}\eta_2{:}\eta_3) = (0.338{:}0.306{:}327)$, $(\eta_1{:}\eta_2{:}\eta_3) = (0.190{:}0.307{:}469)$, and $(\eta_1{:}\eta_2{:}\eta_3{:}\eta_4) = (0.160{:}0.325{:}332{:}0.133)$, and the corresponding theoretical mode purities are $(\eta_1{:}\eta_2{:}\eta_3) = (0.333{:}0.319{:}305)$, $(\eta_1{:}\eta_2{:}\eta_3) = (0.169{:}0.324{:}465)$, and $(\eta_1{:}\eta_2{:}\eta_3{:}\eta_4) = (0.144{:}0.337{:}336{:}0.144)$, respectively. The measured values align well with the theoretical ones, indicating the effectiveness of the design and the successful generation of vortex beams with desired characteristics. The slight differences between the measurement and theoretical results may be caused by the measurement errors and imperfections in the plane wave emitted by the horn antenna. It is worth noting that a bigger metasurface with more meta-atoms is beneficial for generating the multiplexed vortex beams carrying more OAM modes in the practical applications. Considering the maximum four OAM modes carried by the generated multiplexed vortex beams, we choose 10×10 meta-atoms to construct the metasurface proposed in this work to achieve a trade-off between modulation performance and array complexity.

4. CONCLUSION

In conclusion, a space-time-coding metasurface constructed with 1-bit phase coding transmissive meta-atoms for generating the multiplexed vortex beams is presented. Dynamic OAM mode switching is achieved by changing the space-time-coding sequences. Benefitting from the quasi-continuous modulation of the +1st harmonic wave's complex-amplitude, the mode purity of the generated vortex wave is high and the power percentage of each OAM mode can be regulated as expected. The measurement results are in good agreement with the theoretical predictions, demonstrating the effectiveness of the proposed space-time-coding metasurface. Though the prototype metasurface is constructed at microwaves, it is convenient to be generalized to higher frequencies, including terahertz and optics with the space-time-coding method. Furthermore, the proposed metasurface is promising to be applied in the vortex wave multiplexing communication systems.

Funding. National Key Research and Development Program of China (2022YFF0604801); National Natural Science Foundation of China (62271056, 62171186, 62201037); Beijing Natural Science Foundation of China-Haidian Original Innovation Joint Fund (L222042); Open Research Fund of State Key Laboratory of Millimeter Waves (K202326); Open Research Fund of State Key Laboratory of Space-Ground Integrated Information Technology (6142221200201); Basic Research Foundation of Beijing Institute of Technology, China (BITBLR2020014); 111 Project of China (B14010).

Disclosures. The authors declare no conflicts of interest.

Data Availability. Data underlying the results presented in this paper are not publicly available at this time but may be obtained from the authors upon reasonable request.

REFERENCES

1. J. Wang, J. Liu, S. Li, *et al.*, "Orbital angular momentum and beyond in free-space optical communications," Nanophotonics **11**, 645–680 (2022).
2. Y. Guo, S. Zhang, M. Pu, *et al.*, "Spin-decoupled metasurface for simultaneous detection of spin and orbital angular momenta via momentum transformation," Light Sci. Appl. **10**, 63 (2021).
3. J. Liu, J. Zhang, J. Liu, *et al.*, "1-Pbps orbital angular momentum fibre-optic transmission," Light Sci. Appl. **11**, 202 (2022).
4. R. Chen, H. Zhou, M. Moretti, *et al.*, "Orbital angular momentum waves: generation, detection, and emerging applications," Commun. Surveys Tuts. **22**, 840–868 (2020).
5. Z. Liu, S. Gao, Z. Lai, *et al.*, "Broadband, low-crosstalk, and massive-channels OAM modes de/multiplexing based on optical diffraction neural network," Laser Photon. Rev. **17**, 220536 (2023).
6. S. Cai, W. Sheng, and Z. Zhang, "Hybrid channel coding for OAM division multiplexing free space optical communication systems," Opt. Express **31**, 30446–30457 (2023).
7. W. Chen, Q. Lin, W. Chen, *et al.*, "65,536-ary orbital angular momentum–shift keying free-space optical communication based on few-shot learning," Opt. Lett. **48**, 1886–1889 (2023).
8. W. Wang, P. Wang, L. Guo, *et al.*, "Performance investigation of OAMSK modulated wireless optical system over turbulent ocean using convolutional neural networks," J. Lightwave Technol. **38**, 1753–1765 (2020).
9. Z. Zhu, S. Zheng, X. Xiong, *et al.*, "A compact pattern reconfiguration antenna based on multimode plane spiral OA," IEEE Trans. Antennas Propag. **69**, 1168–1172 (2021).
10. Y. Li, M. Jiang, G. Zhang, *et al.*, "Achievable rate maximization for intelligent reflecting surface-assisted orbital angular momentum-based communication systems," IEEE Trans. Veh. Technol. **70**, 7277–7282 (2021).
11. A. H. Tavabi, P. Rosi, A. Roncaglia, *et al.*, "Generation of electron vortex beams with over 1000 orbital angular momentum quanta using a tunable electrostatic spiral phase plate," Appl. Phys. Lett. **121**, 073506 (2022).
12. R. Wang, M. Wang, Y. Zhang, *et al.*, "Generation of orbital angular momentum multiplexing millimeter waves based on a circular traveling wave antenna," Opt. Express **31**, 5131–5139 (2023).
13. A. Valizade Shahmirzadi and A. A. Kishk, "OAM carrying vortex beam mode interconversion using modular cascaded transmitarrays," IEEE Trans. Microwave Theory Tech. **70**, 3591–3605 (2022).
14. S. N. Khonina, A. V. Ustinov, V. I. Logachev, *et al.*, "Properties of vortex light fields generated by generalized spiral phase plates," Phys. Rev. A **101**, 043829 (2020).
15. Y. Yuan, S. Sun, Y. Chen, *et al.*, "A fully phase-modulated metasurface as an energy-controllable circular polarization router," Adv. Sci. **7**, 2001437 (2020).
16. A. Leitis, A. Heßler, S. Wahl, *et al.*, "All-dielectric programmable Huygens' metasurfaces," Adv. Funct. Mater. **30**, 1910259 (2020).
17. L. Dong, L. Si, H. Xu, *et al.*, "Rapid customized design of a conformal optical transparent metamaterial absorber based on the circuit analog optimization method," Opt. Express **30**, 8303–8316 (2022).
18. M. Liu, P. Huo, W. Zhu, *et al.*, "Broadband generation of perfect Poincaré beams via dielectric spin-multiplexed metasurface," Nat. Commun. **12**, 2230 (2021).
19. Q. Xiao, Q. Ma, T. Yan, *et al.*, "Orbital-angular-momentum-encrypted holography based on coding information metasurface," Adv. Opt. Mater. **9**, 2002155 (2021).
20. G. Cheng, L. Si, Q. Shen, *et al.*, "Transmissive Pancharatnam-Berry metasurfaces with stable amplitude and precise phase modulations using dartboard discretization configuration," Opt. Express **31**, 30815–30831 (2023).
21. H. Sroor, Y.-W. Huang, B. Sephton, *et al.*, "High-purity orbital angular momentum states from a visible metasurface laser," Nat. Photonics **14**, 498–503 (2020).
22. S. J. Li, Z. Y. Li, G. S. Huang, *et al.*, "Digital coding transmissive metasurface for multi-OAM-beam," Front. Phys. **17**, 62501 (2022).
23. Y. Wang, K. Zhang, Y. Yuan, *et al.*, "Planar vortex beam generator for circularly polarized incidence based on FSS," IEEE Trans. Antennas Propag. **68**, 1514–1522 (2020).
24. Q. Li, C. Wu, Z. Zhang, *et al.*, "High-purity multi-mode vortex beam generation with full complex-amplitude-controllable metasurface," IEEE Trans. Antennas Propag. **71**, 774–782 (2023).
25. Y. Li, J. Lin, H. Guo, *et al.*, "A tunable metasurface with switchable functionalities: from perfect transparency to perfect absorption," Adv. Opt. Mater. **8**, 1901548 (2020).
26. Q. Li, M. Gupta, X. Zhang, *et al.*, "Active control of asymmetric Fano resonances with graphene–silicon-integrated terahertz metamaterials," Adv. Mater. Technol. **5**, 1900840 (2020).
27. P. Tang, L. Si, L. Dong, *et al.*, "Tunable broadband terahertz graphene metasurface for complex-amplitude vortex beam generator and hologram," Opt. Laser Technol. **175**, 110874 (2024).
28. Q. Ma, Q. R. Hong, X. X. Gao, *et al.*, "Smart sensing metasurface with self-defined functions in dual polarizations," Nanophotonics **9**, 3271–3278 (2020).
29. X. Bai, F. Zhang, L. Sun, *et al.*, "Dynamic millimeter-wave OAM beam generation through programmable metasurface," Nanophotonics **11**, 1389–1399 (2022).
30. X. Bai, F. Kong, Y. Sun, *et al.*, "High-efficiency transmissive programmable metasurface for multimode OAM generation," Adv. Opt. Mater. **8**, 2000570 (2020).
31. Y. Hu, S. N. Chen, Y. Shi, *et al.*, "Space-time coding metasurface for multifunctional holographic imaging," Adv. Mater. Technol. **9**, 2302164 (2024).
32. R. Feng, B. Ratni, J. Yi, *et al.*, "Versatile metasurface platform for electromagnetic wave tailoring," Photon. Res. **9**, 1650–1659 (2021).
33. J. Y. Dai, L. X. Yang, J. C. Ke, *et al.*, "High-efficiency synthesizer for spatial waves based on space-time-coding digital metasurface," Laser Photon. Rev. **14**, 1900133 (2020).
34. Q. Hu, W. Yang, J. Wang, *et al.*, "Dynamically generating diverse multi-beams with on-demand polarizations through space-time coding metasurface," Adv. Opt. Mater. **12**, 2300093 (2023).
35. L. Zhang, X. Chen, S. Liu, *et al.*, "Space-time-coding digital metasurfaces," Nat. Commun. **9**, 4334 (2018).
36. J. Yang, J. C. Ke, M. Chen, *et al.*, "Control of the harmonic near-field distributions by an active metasurface loaded with pin diodes," Photon. Res. **9**, 344–350 (2021).
37. H. Wu, X. X. Gao, L. Zhang, *et al.*, "Harmonic information transitions of spatiotemporal metasurfaces," Light: Sci. Appl. **9**, 198 (2020).
38. L. Zhang, M. Z. Chen, W. Tang, *et al.*, "A wireless communication scheme based on space- and frequency-division multiplexing using digital metasurfaces," Nat. Electron. **4**, 218–227 (2021).
39. S. Taravati and G. V. Eleftheriades, "Microwave space-time-modulated metasurfaces," ACS Photon. **9**, 305–318 (2022).
40. V. Bruno, C. DeVault, S. Vezzoli, *et al.*, "Negative refraction in time-varying strongly coupled plasmonic-antenna–epsilon-near-zero systems," Phys. Rev. Lett. **124**, 043902 (2020).
41. D. Ramaccia, D. L. Sounas, A. Alu, *et al.*, "Phase-induced frequency conversion and Doppler effect with time-modulated metasurfaces," IEEE Trans. Antennas Propag. **68**, 1607–1617 (2020).
42. H. N. Bui, N. H. Phi, A. Alsaadi, *et al.*, "Space–time-modulated reconfigurable metamaterial based on a field-focused cavity for nonreciprocal transmission control and frequency conversion," ACS Appl. Mater. Interfaces **14**, 26931–26940 (2022).
43. J. Park, B. G. Jeong, S. I. Kim, *et al.*, "All-solid-state spatial light modulator with independent phase and amplitude control for three-dimensional LiDAR applications," Nat. Nanotechnol. **16**, 69–76 (2021).
44. C. Meng, P. C. V. Thrane, F. Ding, *et al.*, "Dynamic piezoelectric MEMS-based optical metasurfaces," Sci. Adv. **7**, eabg5639 (2021).
45. J. Zhang, Y. Kosugi, M. Ogasawara, *et al.*, "High-speed metasurface modulator using perfectly absorptive bimodal plasmonic resonance," APL Photon. **8**, 121304 (2023).
46. W. Yang, K. Chen, Y. Zheng, *et al.*, "Angular-adaptive reconfigurable spin-locked metasurface retroreflector," Adv. Sci. **8**, 2100885 (2021).
47. R. Zhu, J. Wang, C. Ding, *et al.*, "Multi-field-sensing metasurface with robust self-adaptive reconfigurability," Nanophotonics **12**, 1337–1345 (2023).
48. S. C. Malek, H.-S. Ee, and R. Agarwal, "Strain multiplexed metasurface holograms on a stretchable substrate," Nano Lett. **17**, 3641–3645 (2017).

49. Y. Meng, Z. Liu, Z. Xie, *et al.*, "Versatile on-chip light coupling and (de) multiplexing from arbitrary polarizations to controlled waveguide modes using an integrated dielectric metasurface," Photon. Res. **8**, 564–576 (2020).
50. Z. Xie, T. Lei, F. Li, *et al.*, "Ultra-broadband on-chip twisted light emitter for optical communications," Light: Sci. Appl. **7**, 18001 (2018).
51. J. Wang, J.-Y. Yang, I. M. Fazal, *et al.*, "Terabit free-space data transmission employing orbital angular momentum multiplexing," Nat. Photonics **6**, 488–496 (2012).
52. G. Naik, J. Liu, and J.-M. J. Park, "Coexistence of wireless technologies in the 5 GHz bands: a survey of existing solutions and a roadmap for future research," Commun. Surveys Tuts. **20**, 1777–1798 (2018).